Available online at www.sciencedirect.com

jmr&t
Journal of Materials Research and Technology

journal homepage: www.elsevier.com/locate/jmrt

Original Article

On the low temperature creep controlling mechanism in a high strength spring steel

Nagarjuna Remalli [a,*], *Mathias Münch* [b], *Mohsin Hasan* [c], *K Nanda Kishore* [c], *Felix Stern* [d], *Nikolas Baak* [d], *Frank Walther* [d], *Manjini Sambandam* [e], *Steffen Klapprott* [f], *Koteswararao V. Rajulapati* [c], *Robert Brandt* [a]

[a] *University of Siegen, Chair for Lightweight Construction for Automotive, Siegen, 57076, North Rhine Westphalia, Germany*
[b] *Mubea Motorkomponenten GmbH, Material Engineering Valve Springs, Attendorn, 57439, North Rhine Westphalia, Germany*
[c] *University of Hyderabad, School of Engineering Sciences and Technology (SEST), Hyderabad, 500046, Telangana, India*
[d] *TU Dortmund University, Chair of Materials Test Engineering, Dortmund, 44227, North Rhine Westphalia, Germany*
[e] *JSW Steel Ltd. Salem Works, Salem, 636453, Tamilnadu, India*
[f] *Mubea Fahrwerksfedern GmbH, Quality and Material Development Chassis, Weissensee, 99631, Thueringen, Germany*

ARTICLE INFO

Article history:
Received 1 July 2022
Accepted 21 September 2022
Available online 14 October 2022

Keywords:
Martensitic steel
Low temperature creep
Exhaustion creep model
Dislocation glide
Slip localization
Strain induced phase transformation

ABSTRACT

Despite of the well-known fact that high strength steels are exhibiting low temperature creep deformation, its rate controlling mechanism is yet to be understood. The strain hardening theory and the exhaustion creep model were proposed almost seven decades ago to unravel the low temperature creep mechanism in a single phase homogeneous isotropic material. However, their applicability to low temperature creep deformation in a technical material like a modern high strength steel is still a matter of investigation owing to their nature of multi-phase, in-homogeneous, and an-isotropic behavior. The authors have grabbed this chance to experimentally validate the exhaustion creep model based on low temperature creep tests of the SAE 9254 spring steel. The ultimate tensile strength and yield strength σ_e of SAE 9254 were determined in a temperature range of $298\ K \leq T \leq 353\ K$ at a constant strain rate of $2.5 \bullet 10^{-4}\ s^{-1}$. Low temperature creep deformation behavior was studied at the above-mentioned temperatures T at a constant stress $\sigma = 1634\ MPa$, and at stresses $1071\ MPa \leq \sigma \leq 1634\ MPa$ at a constant temperature $T = 353\ K$ for a duration of 1 *hr*, respectively, at each condition. The retained austenite quantity was determined prior and post low temperature creep testing by means of X-ray diffraction. A reworked exhaustion creep model well describes the stress σ and temperature T dependency of low temperature creep deformation behavior in SAE 9254. Consequently, our hypothesis of a low temperature creep rate controlling mechanism reads: Low temperature creep strain is predominantly contributed by dislocation glide in the retained austenite phase. The reduction in

* Corresponding author.
E-mail address: nagarjuna.remalli@uni-siegen.de (N. Remalli).
https://doi.org/10.1016/j.jmrt.2022.09.131
2238-7854/© 2022 The Authors. Published by Elsevier B.V. This is an open access article under the CC BY-NC-ND license (http://creativecommons.org/licenses/by-nc-nd/4.0/).

creep rate with time can then be attributed to the exhaustion of this specific deformation mechanism by strain induced martensitic transformation of the retained austenite.
© 2022 The Authors. Published by Elsevier B.V. This is an open access article under the CC BY-NC-ND license (http://creativecommons.org/licenses/by-nc-nd/4.0/).

1. Introduction

The usage of advanced high strength steels (HSS) in automotive components, e.g., suspension coil springs, prevailed owing to their superior mechanical properties. The increase in global awareness urges automotive industries to focus on further weight reduction to reduce the fuel consumption, which leads to higher stresses acting on the spring material. Consequently, the spring material is prone to undergo low temperature creep (LTC) deformation that would affect the intended function of the coil spring. LTC is defined as the time dependent deformation at a constant stress σ that is less than the yield strength (YS) σ_e ($\sigma < \sigma_e$) and at a constant temperature T that is lower than the melting temperature T_m ($T < 0.3 \bullet T_m$). Ample amount of LTC investigations on a wide range of materials, e.g., Ti-alloys [1–3], stainless steel [4,5], pipeline steel [6], Cu [7], and pure Al [8] have been performed over the last three decades, which are summarized by Kassner et al. [9]. However, LTC investigations confined to HSS, especially under the restricted conditions of $\sigma < \sigma_e$ and $T < 0.3 \bullet T_m$, are limited [10–13] and these results were suggesting that LTC strain $\varepsilon_{cr}(t)$ of HSS follows a logarithmic creep law

$$\varepsilon_{cr}(t) = \alpha \bullet \ln(\beta \bullet t + 1) \tag{1}$$

where $\alpha(\sigma, T)$ and $\beta(\sigma, T)$ are material specific creep parameters.

Liu et al. [13] studied the impact of varying small amounts of a secondary phase, i.e. ferrite, on room temperature creep behaviour of SAE 4340 multi-phase steel. Samples having the same YS σ_e of 1280 ± 10 *MPa* but different ferrite contents of 0–4% exhibit a time dependent room temperature creep strain $\varepsilon_{cr}(t)$ that follows a logarithmic creep law. Furthermore, the increase in LTC strain $\varepsilon_{cr}(t)$ with increasing ferrite content was attributed to the hypothesis of slip localization mainly in the softer ferrite phase [13]. Neu et al. [10] reported the stress σ and temperature T dependency of the LTC strain in the carburized 4320 steel having a martensitic matrix with 14 – 35% of retained austenite (RA). Their experiments revealed that two deformation modes are contributing to the total strain under constant load, one is creep strain and the other one is volumetric transformation strain due to the martensitic transformation of RA. According to them, RA transformation could be aided by either thermal induced or stress assisted martensitic transformation depending on the test temperature T. Irrespective of the contributing mechanism, they reported that the creep strain follows a logarithmic creep law. Alfredsson et al. [14] investigated the stress σ and temperature T dependency of the LTC behavior of the roller bearing steel grade 100CrMnMo8. They reported that LTC strain $\varepsilon_{cr}(t)$ obeys a logarithmic creep law in material with a bainitic matrix. On the other hand, LTC strain $\varepsilon_{cr}(t)$ in the same steel grade with a martensitic matrix follows a power law [14]. Furthermore, they address the occurrence of RA phase transformation under tensile loading in terms of the strength differential effect (SDE) in their LTC models for a good correlation with experimental data.

A mechanism based exhaustion creep model (ECM) was proposed by Nabarro et al. [15,16], and Smith [17] to explicate the logarithmic creep behavior. It considers that LTC strain is contributed by dislocation glide in a single phase, homogeneous, isotropic material. However, Nabarro's original version is incapable of describing the above mentioned the stress σ and temperature T dependency of LTC strain and, thus, it does not disclose the LTC rate controlling mechanism. Hence, the authors have reworked his ECM (unpublished data), and the prominent modifications are summarized as follows:

Nabarro assumed that the material has a wide range of obstacles characterized by their activation stress σ_i between $0 - \infty$ *Pa*. Besides, he assumed an obstacle distribution function $\varphi\, d\sigma$ as a slowly varying function of stress σ. To explain the reduction in creep rate $\dot{\varepsilon}_{cr}(t)$ during creep, an obstacle can be surmounted by a dislocation only once followed by its exhaustion [15].

In the reworked ECM, the authors consider only those obstacles with an activation stress up to the YS σ_e. As a matter of that, a stress dependent obstacle distribution function $\varphi(\sigma)$ has been introduced in the reworked ECM. Besides, we allow a dislocation to overcome obstacles more than once, i.e. multiple times n, before it gets exhausted, e.g., by phase transformation. The function $n = n(T)$ is considered as temperature T dependent. With these modifications, LTC strain $\varepsilon_{cr}(t)$ reads:

$$\varepsilon_{cr}(t) = \alpha^E \bullet \left[\ln\left(\frac{f_0^*}{f_1^*}\right) + E_1(f_0^* \bullet t) - E_1(f_1^* \bullet t) \right] \tag{2}$$

with $E_1(x)$ being an exponential integral function [18] and

$$\alpha^E(\sigma, T) = C \bullet \frac{\sigma_e}{(\sigma_e - \sigma)^2} \bullet T \bullet n(T) \tag{3}$$

$$f_0^*(T) = \frac{f_0}{n(T)} \text{ and } f_1^*(\sigma, T) = f_0^*(T) \bullet exp\left[-\frac{v_e \bullet (\sigma_e - \sigma)}{k \bullet T} \right] \tag{4}$$

$$n(T) = \frac{f_0}{f_0^*(T)} \text{ and } \frac{f_1^*(\sigma, T)}{f_0^*(T)} = exp\left[-\frac{v_e \bullet (\sigma_e - \sigma)}{k \bullet T} \right] \tag{5}$$

with C being a materials constant, v_e being the mean activation volume of the here considered obstacles, and k being the Boltzmann constant. The creep parameters $n(T)$, $\alpha^E(\sigma, T)$, and

Table 1 – Chemical composition of SAE 9254 (in wt.%) provided by the material supplier.

C	Si	Mn	Cr	Fe
0.53	1.32	0.69	0.71	Bal.

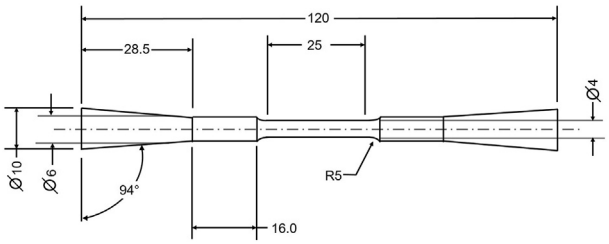

Fig. 1 – Tensile and LTC specimen dimensions in mm.

$f_1^*(\sigma,T)/f_0^*(T)$ are functions of stress σ and temperature T with f_0 being a frequency with which the dislocation attempts to overcome an obstacle. Consequently, the LTC strain $\varepsilon_{cr}(t)$ follows a non-logarithmic creep behavior (Eq. (2)) according to the reworked ECM.

The primary interest of the current study on high strength martensitic steel is to take a significant step to disclose the LTC creep rate controlling mechanism in high strength martensitic steel. Thus, our mechanism based reworked ECM must be verified in a multi-stage procedure. Firstly, the non-logarithmic creep law is applied by best fitting of Eqn 2 to the LTC strain data of SAE 9254. Subsequently, the creep parameters $n(T)$, $\alpha^E(\sigma, T)$, and $f_1^*(\sigma,T)/f_0^*(T)$ ought to represent the stress σ and temperature T dependency of LTC strain correctly. Their fitting parameters σ_e and v_e must be validated. Eventually, the authors formulate a hypothesis of the LTC rate controlling mechanism by correlating the macroscopic LTC deformation of SAE 9254 to changes in RA content on a microscopic scale.

2. Experimental details

SAE 9254 (see Table 1) wire rods of 12 *mm* diameter supplied in hot rolled condition were "Inductive quenched and tempered (IQT)" at Mubea Fahrwerksfedern GmbH, Weissensee, Germany. The heat treatment parameters are not disclosed here. Tensile and LTC tests were performed under uni-axial loading followed by phase quantification by means of XRD. Specimens for tensile and LTC testing were fabricated along the rolling direction with a gauge length $l = 25\ mm$ and gauge diameter $d = 4\ mm$, respectively as shown in Fig. 1.

The tensile tests as well as the LTC tests were performed by means of the universal testing system Shimadzu AG-X equipped with a 100 *kN* load cell. The system is used in combination with a thermostatic chamber. Strain measurement was realized by using the high resolution digital image correlation (DIC) system Limess Q400 with two cameras for 3D-evaluation of each specimen's surface. A DIC speckle pattern was applied by priming the specimen's surface with a special heat resistant black paint. Subsequently, a white paint in the form of randomly distributed dots was applied. Pictures for correlation were taken time-triggered every 0.5 *s* and 5 *s* for tensile and LTC tests, respectively. Creep strain $\varepsilon_{cr}(t)$ was measured by using the evaluation software Istra 4D, which allows to apply a virtual gauge line element on the specimen in longitudinal or test load direction.

Ultimate Tensile Strength (UTS) and YS σ_e were determined at temperatures $298\ K \leq T \leq 353\ K$ with a constant strain rate of $2.5 \bullet 10^{-4}\ s^{-1}$. Three specimens were tested at each condition, respectively. LTC deformation behavior was studied at the above-mentioned temperatures T at a constant stress $\sigma = 1634\ MPa$, and at stresses $1071\ MPa \leq \sigma \leq 1634\ MPa$ at a constant temperature $T = 353\ K$ for a duration of 1 *hr*, respectively, at each condition. Two specimens were tested at each condition to confirm reproducibility of the results. The loading was applied at a constant rate of 500 N/s, respectively, until achieving the required creep load. The creep strain $\varepsilon_{cr}(t)$ is then defined by the change of total strain $\varepsilon(t)$ compared to the instantaneous strain ε_0 after achieving the creep load [11]

$$\varepsilon_{cr}(t) = \varepsilon(t) - \varepsilon_0 \tag{6}$$

For a quantitative phase analysis prior to LTC, samples are sectioned from the IQT wire rod. Subsequently, the samples were grounded with silicon carbides abrasive papers of grit size up to 1200, then polished with diamond paste having particle

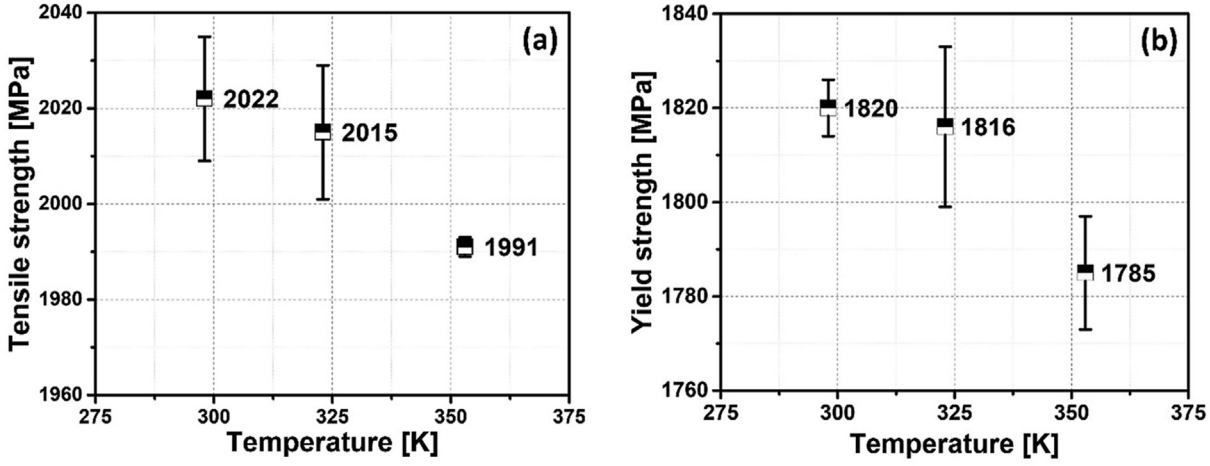

Fig. 2 – Temperature dependence of (a) Tensile strength, (b) Yield strength of IQT. The average values are given in each diagram, respectively.

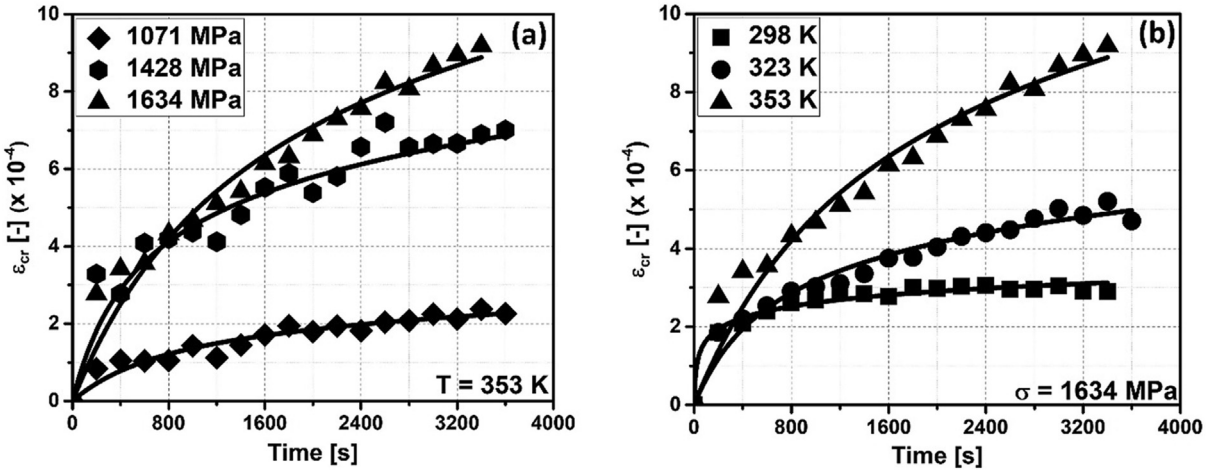

Fig. 3 – (a) Stress dependency of LTC behaviour at a constant temperature $T = 353\,K$, (b) Temperature dependency of LTC behaviour at a constant stress $\sigma = 1634\,MPa$.

sizes 6, 3, and 1 μm. For a quantitative phase analysis after LTC, specimens from the middle of the gauge section have been considered. An empyrean Panalytical X-ray diffractometer operated at 40 kV and 30 mA with $Cr-K\alpha$ monochromatic source and V $k\beta$ filter having 0.02 thickness was used to record the pattern in $70^\circ \leq 2\theta \leq 162^\circ$ with a step size of 0.026° and step time of 10 s. The {200}, {220} peaks of RA and {200} peak of martensite were considered for the RA quantity determination according to SAE 453 method [19].

3. Experimental results

The IQT steel has a $UTS = 2022\,MPa$ and $\sigma_e = 1820\,MPa$ at 298 K, respectively. UTS and σ_e decreases with increasing temperature up to 353 K slightly as shown in Fig. 2. The creep strain data at regular intervals of 200 s each are presented in Fig. 3(a) and (b) by individual symbols for the considered stress σ and temperature T levels, respectively. Fig. 3(a) shows experimentally measured LTC strain at stresses $1071\,MPa \leq \sigma \leq 1634\,MPa$ at a constant temperature $T = 353\,K$, and Fig. 3(b) shows experimentally measured LTC strain at $298\,K \leq T \leq 353\,K$ at a constant stress $\sigma = 1634\,MPa$. It is evident that the $\varepsilon_{cr}(t)$ increases with increasing stress σ and temperature T at a given time t. The experimental data, which have been fitted according to the creep law (Eq. (2)), are represented by solid lines in Fig. 3. The ECM creep law fits well with all the experimental LTC strain data with a coefficient of determination of $R^2 \geq 0.92$. The creep parameters α^E, f_0^*, and f_1^* by best fitting of the experimental data are shown in Table 2.

With Eq. (5), the relative number $n(T)/n(T=T_0)$ of activation reads

$$\frac{n(T)}{n(T=T_0)} = \frac{f_0^*(T=T_0)}{f_0^*(T)} \tag{7}$$

Fig. 4 shows that it increases linearly with temperature T. By best fitting it becomes

$$\frac{n(T)}{n(T=T_0)} = a \bullet (T-T_0) + 1 \tag{8}$$

with fitting parameters, $a = 2.274\,K^{-1}$ and $T_0 = 298\,K$, respectively. Subsequently, $\alpha^E, f_1^*/f_0^*$ have been fitted in 3D surface fit by means of fitting functions according to Eqs. (3) and (5). For convenience, these fits are here shown in 2D plots (see Fig. 5, Fig. 6). Fig. 5(a, b) show the stress dependence of the creep parameter α_T^E at a constant temperature $T = 353\,K$ and the temperature dependence of the creep parameter α_σ^E at a constant stress $\sigma = 1634\,MPa$, respectively. The creep parameter α^E increases with increasing stress σ and temperature T. It is well described by Eq. (3) according to the reworked ECM with a coefficient of determination of $R^2 = 0.96$ as shown in Fig. 5. The fitting parameters C, σ_e are determined as 0.9842 Pa and 2160 MPa, respectively. Fig. 6(a, b) show the stress dependence of $f_1^*/f_0^*|_T$ at a constant temperature $T = 353\,K$ and the temperature dependence of $f_1^*/f_0^*|_\sigma$ at a constant stress $\sigma =$

Table 2 – The creep parameters α^E, f_0^*, and f_1^* by best fitting of the experimental LTC data.

Stress [MPa]	Temperature [K]	α^E ($\bullet 10^{-4}$) [–]	f_0^* ($\bullet 10^{-3}$) [s^{-1}]	f_1^* ($\bullet 10^{-13}$) [s^{-1}]	R^2
1071	353	0.70	3.88	2.43	0.93
1428	353	1.82	6.69	1.77	0.92
1634	353	3.38	2.29	14.09	0.96
1634	323	1.40	5.41	1.06	0.97
1634	298	0.43	288.13	0.084	0.97

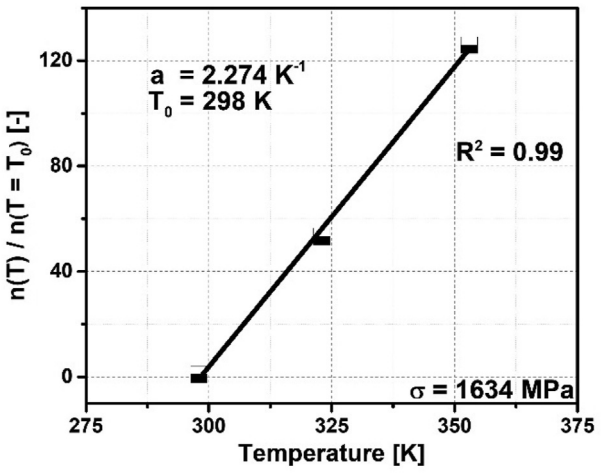

Fig. 4 – Temperature dependence of $n(T)/n(T = T_0)$ at a constant stress $\sigma = 1634$ MPa.

1634 MPa, respectively. The stress σ and temperature T dependence of f_1^*/f_0^* is well described by Eq. (5) according to the reworked ECM with a coefficient of determination of $R^2 = 0.97$. The fitting parameter v_e is determined as $1.96 \bullet 10^{-28}\ m^3$. It is evident that the reworked ECM fits well to the stress σ and temperature T dependence of creep parameters $\alpha^E, f_1^*/f_0^*$, and, consequently, describes the LTC behaviour of the investigated spring steel quite well.

Fig. 7 shows the average RA content in IQT steel rods prior and post LTC testing performed within $298\ K \leq T \leq 353\ K$ at a constant stress $\sigma = 1634$ MPa. The RA content in the IQT rod is 8.9% which is considered as a reference, whereas the RA quantities in the deformed LTC specimens are about 7.6% irrespective of the test temperature.

4. Discussion

Our reworked ECM is capable to describe LTC strain $\varepsilon_{cr}(t)$ in IQT steel SAE 9254 and the stress σ and temperature T dependence of the creep parameters $n(T)$, $\alpha^E(\sigma, T)$, and $f_1^*(\sigma, T)/f_0^*(T)$ as shown in Fig. 4, Fig. 5, and Fig. 6, respectively. The value of σ_e is determined by fitting α^E with respect to stress σ and temperature T as 2160 MPa, which is in the expected range of YS σ_e of the investigated IQT steel. The mean activation volume v_e in Eq. (5) is determined by fitting f_1^*/f_0^* with respect to stress σ and temperature T as $1.96 \bullet 10^{-28}\ m^3$ that is equal to $12 \bullet b^3$ with the burgers vector b of the most favorable slip system in austenite phase, i.e. (111)[110]. As reported by Conrad [20], the magnitude of activation volume indicates overcoming the Peierls-Nabarro stress as the mechanism for dislocation motion. Since the activation volume v_e of $12 \bullet b^3$ for LTC strain here in the considered stress σ and temperature T is determined by the consideration of the most favorable slip system in austenite phase, the authors proposed by strictly following the work of Neu et al. [10], and Alfredsson et al. [14], that this LTC strain is contributed by slip localization within RA in SAE 9254. It is evident from Fig. 4 that the relative number $n(T)/n(T = T_0)$ of multiple activations of a dislocation before exhaustion increases with temperature T during LTC deformation. The fitting parameter T_0 in Eq. (8) is determined as 298 K. It indicates that the dislocation activation ceases below ambient temperature, which is plausible to consider. Fig. 8 shows the normalized creep rate $\dot{\varepsilon}_{cr}(t)/\dot{\varepsilon}_{cr}(t = 0)|_\sigma$ as a function of time t for three different temperatures T. The drop-in normalized creep rate $\dot{\varepsilon}_{cr}(t)/\dot{\varepsilon}_{cr}(t = 0)|_\sigma$ with time t might be attributed to the exhaustion of dislocation glide within RA due to strain induced martensitic transformation (SIMT). As postulated in [21,22], multiple slip activations, majorly at two intersecting {111} type slip bands, led to nucleation of cubic α' martensite in metastable austenite. It is evident from Fig. 7 that the RA content dropped

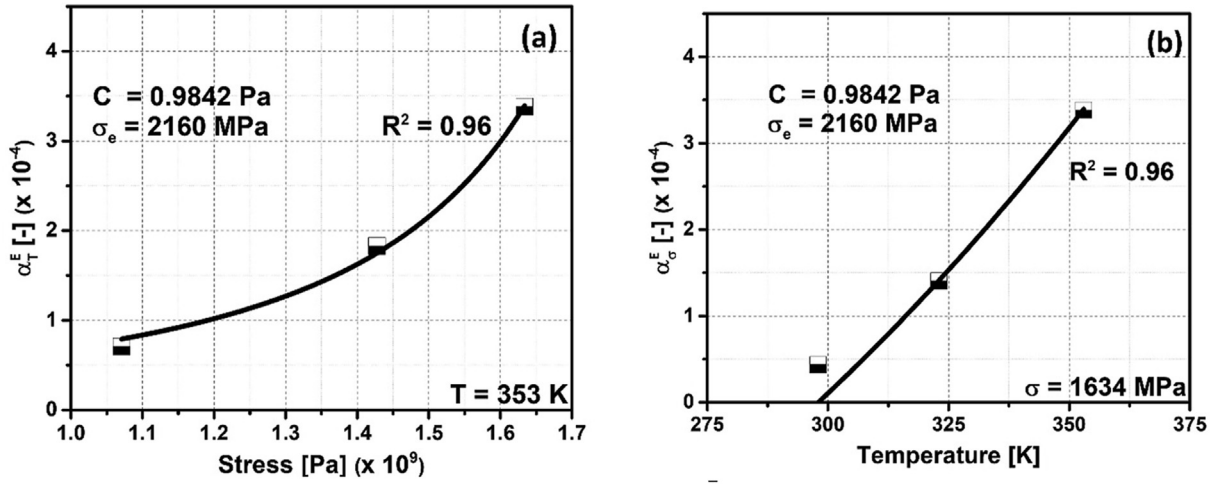

Fig. 5 – (a) Stress dependence of creep parameter α_T^E at a constant temperature $T = 353$ K, (b) Temperature dependence of creep parameter α_σ^E at a constant stress $\sigma = 1634$ MPa.

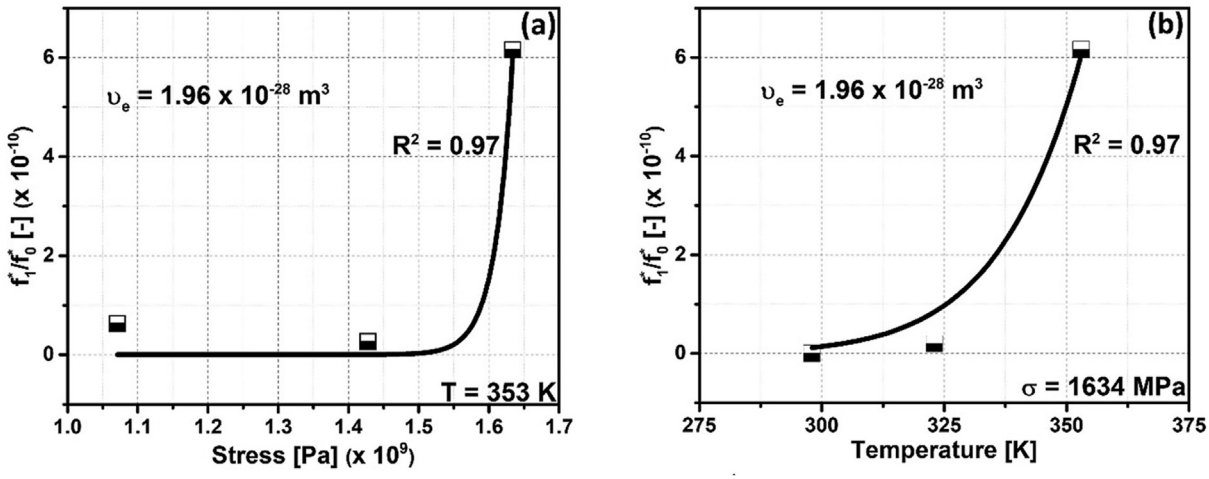

Fig. 6 – (a) Stress dependence of creep parameter $f_1^*/f_0^*|_T$ at a constant temperature $T = 353$ K, (b) Temperature dependence of creep parameter $f_1^*/f_0^*|_\sigma$ at a constant stress $\sigma = 1634$ MPa.

by 15% of its initial amount during LTC deformation irrespective of the test temperature *T*, which might be due to the occurrence of *SIMT* locally in the deformed *RA*. Furthermore, the drop-in normalized creep rate $\dot{\varepsilon}_{cr}(t)/\dot{\varepsilon}_{cr}(t=0)|_\sigma$ becomes sluggish at elevated temperatures *T*. As shown in Fig. 8 inset, the creep rate $\dot{\varepsilon}_{cr}(t)$ dropped to 20% of its initial values in less than 200 *s* at 298 *K*, whereas this time *t* is higher for 353 *K*. The relation between $\ddot{\varepsilon}_{cr}(t)$ and $n(T)$ for the short time interval is derived from Eqs. (3) and (4) as

$$\ddot{\varepsilon}_{cr}(t) = -\alpha^E \bullet \frac{f_0^2}{2} \bullet \frac{1}{n^2(T)} \tag{9}$$

One can realize from Eq. (9) that the rate of drop-in creep rate $\dot{\varepsilon}_{cr}(t)$ is inversely proportional to $n^2(T)$. As shown in Fig. 4, $n(T)$ increases linearly with temperature *T*. Consequently, the rate of drop-in creep rate $\dot{\varepsilon}_{cr}(t)$ can be considered as inversely proportional to T^2, which indicates that the rate of drop-in $\dot{\varepsilon}_{cr}(t)$ becomes sluggish at elevated temperatures *T*, for a given time *t*. This can be justified in terms of austenite stability. As reported by Neu et al. [23], the stability of austenite increases with temperature *T*. As the *RA* stability increases, there would be high chances for multiple activations of dislocation within *RA* prior to its transformation into martensite. Based on these experimental results, our hypothesis of LTC mechanism implies that LTC strain $\varepsilon_{cr}(t)$ in IQT steel SAE 9254 is contributed by slip localization within *RA*, whereas reduction in creep rate is controlled by *SIMT*, which might be occurring locally in the deformed *RA*. An experimental

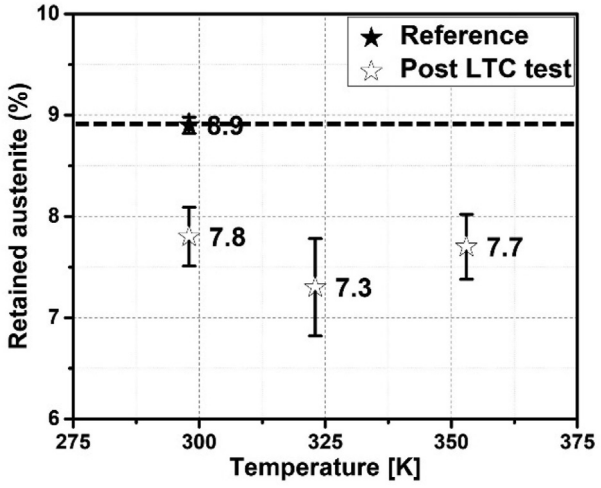

Fig. 7 – RA determination prior and post LTC testing performed at 298 $K \leq T \leq$ 353 *K* a constant stress $\sigma = 1634$ MPa.

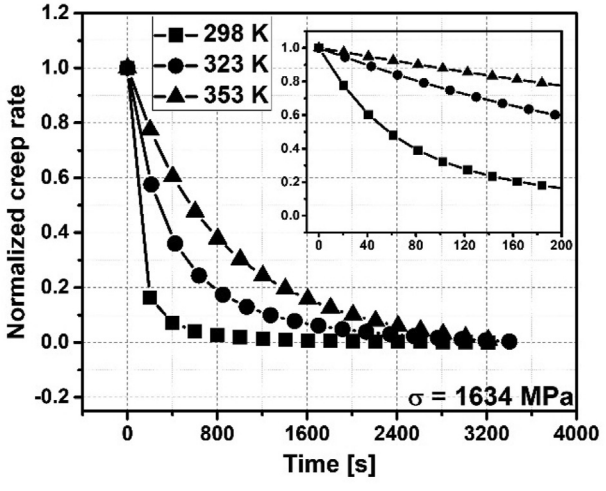

Fig. 8 – Time and temperature dependence of normalized creep rate $\dot{\varepsilon}_{cr}(t)/\dot{\varepsilon}_{cr}(t=0)|_\sigma$ for LTC tests performed at 298 $K \leq T \leq$ 353 *K* and at a constant stress $\sigma = 1634$ MPa. Inset: Details are shown for short time interval, i.e. up to 200 *s*.

proof of the here presented hypothesis, e.g., by means of TEM investigations, is still due. Therefore, the authors encourage and appreciate support in this subject.

5. Conclusions

The main results of the current study presented are as follows:

- Our reworked ECM is capable to describe LTC strain $\varepsilon_{cr}(t)$ behavior in IQT steel SAE 9254.
- Furthermore, the stress σ and temperature T dependence of the creep parameters $n(T)$, $\alpha^{E}(\sigma,T)$, and $f_1^*(\sigma,T)/f_0^*(T)$ can be well justified in terms of the reworked ECM.
- The value of σ_e is determined by fitting α^{E} with respect to stress σ and temperature T as 2160 *MPa*, which is close to the YS σ_e of the investigated IQT steel.
- The mean activation volume v_e is determined by fitting f_1^*/f_0^* with respect to stress σ and temperature T as $1.96 \bullet 10^{-28}\ m^3$, which indicates that LTC strain is contributed by slip localization possibly, within *RA*.
- The *RA* content dropped by 15% of its initial amount during LTC deformation irrespective of the test temperature T, which might be due to the occurrence of *SIMT* locally in the deformed *RA*.
- Hence, the drop-in creep rate $\dot{\varepsilon}_{cr}(t)$ with time could be attributed to the exhaustion of the dislocation glide mechanism within deformed *RA* due to *SIMT*. An experimental proof of the here presented hypothesis is still due.
- The rate of drop-in creep rate $\dot{\varepsilon}_{cr}(t)$ becomes sluggish at elevated temperatures T, for a given time t, which can be justified in terms of austenite stability at elevated temperatures.
- Based on these experimental results, our hypothesis on the LTC rate controlling mechanism in SAE 9254 implies that LTC strain is contributed by slip localization within *RA*, whereas the reduction in creep rate is controlled by *SIMT*.

Declaration of Competing Interest

The authors declare that they have no known competing financial interests or personal relationships that could have appeared to influence the work reported in this paper.

Acknowledgements

The financial support received from “Indo-German Science and Technology Centre (IGSTC)” under the grant no.: 01DQ19006A is gratefully acknowledged. A part of this work was performed at the “Micro- and Nanoanalytics Facility (MNaF)” of the University of Siegen.

REFERENCES

[1] Miller WH, Chen RT, Starke EA. Microstructure, creep, and tensile deformation in Ti-6Al-2Nb-1Ta-0.8Mo. Metall Mater Trans 1987;18(8):1451–68.
[2] Neeraj T, Hou DH, Daehn GS, Mills MJ. Phenomenological and microstructural analysis of room temperature creep in titanium alloys. Acta Mater 2000;48(6):1225–38.
[3] Kameyama T, Matsunaga T, Sato E, Kuribayashi K. Suppression of ambient-temperature creep in CP-Ti by cold-rolling. Mat Sci Eng. A 2009;510-511:364–7.
[4] Alden TH. Strain hardening during low temperature creep of 304 stainless steel. Acta Metall 1987;35(11):2621–6.
[5] Kassner ME, Geantil P, Rosen RS. Ambient temperature creep of type 304 stainless steel. J Eng Mater Technol 2011;133(2).
[6] Wang SH, Zhang Y, Chen W. Room temperature creep and strain-rate-dependent stress-strain behavior of pipeline steels. J Mater Sci 2001;36(8):1931–8.
[7] Yen C, Caulfield T, Roth LD, Wells JM, Tien JK. Creep of copper at cryogenic temperatures. Cryogenics 1984;24(7):371–7.
[8] Shen J, Yamasaki S, Ikeda K, Hata S, Nakashima H. Low-temperature creep at ultra-low strain rates in pure aluminum studied by a helicoid spring specimen technique. Mater Trans 2011;52(7):1381–7.
[9] Kassner ME, Smith K. Low temperature creep plasticity. J Mater Res Technol 2014;3(3):280–8.
[10] Neu RW, Sehitoglu H. Low-temperature creep of a carburized steel. Metall Trans A 1992;23(9):2619–24.
[11] Oehlert A, Atrens A. Room temperature creep of high strength steels. Acta Metall Mater 1994;42(5):1493–508.
[12] Liu C, Zhao Z, Northwood DO. Effect of heat treatments on room temperature creep strain of a high strength steel. KEM 2000;171-174:403–10.
[13] Liu C, Bhole S, Northwood DO. The effects of ferrite content and morphology on the mechanical properties and room temperature creep of quenched and tempered SAE 4340 steel. JSME Int J Ser A Solid Mech Mat Eng 2003;46(3):272–7.
[14] Alfredsson B, Arregui IL, Lai J. Low temperature creep in a high strength roller bearing steel. Mech Mater 2016;100:109–25.
[15] Nabarro FR. Theory of crystal dislocations Oxford. Clarendon; 1967.
[16] Nabarro FR. The time constant of logarithmic creep and relaxation. Mat Sci Eng. A 2001;309-310:227–8.
[17] Smith CL. A Theory of Transient Creep in Metals 1948;61:201–5.
[18] Abramowitz M, Stegun IA. Handbook of mathematical functions: with formulas, graphs and mathematical tables. In: Milton Abramowitz and Irene A. Stegun. New York: Wiley; 1972.
[19] Jatczak CF, editor. Retained austenite and its measurement by X-ray diffraction. Warrendale, PA, United States: SAE International400 Commonwealth Drive; 1980.
[20] Conrad H. Thermally activated deformation of metals. J Occup Med 1964;16(7):582–8.
[21] Krupp U, Roth I, Christ HJ, Kuebbeler M, Fritzen CP, editors. On the mechanism of martensite formation during short fatigue crack propagation in austenitic stainless steel. Experimental Identification and Modelling Concept; 2013.
[22] Olson GB, Cohen M. Kinetics of strain-induced martensitic nucleation. Metall Mater Trans 1975;6(4):791–5.
[23] Neu RW. An investigation into the mechanisms of cone bore growth in railroad bearings. University of Illinois at Urbana-Champaign; 1991.